[5] Singh, A., & Kostova, I. (2024). Health effects of heavy metal contaminants Vis-à-Vis microbial response in their bioremediation. *Inorganica Chimica Acta*, *568*, 122068.

[6] Antoine, J. M., Fung, L. A. H., & Grant, C. N. (2017b). Assessment of the potential health risks associated with the aluminium, arsenic, cadmium and lead content in selected fruits and vegetables grown in Jamaica. *Toxicology Reports*, *4*, 181.

[7] Emmanuel, U. C., Chukwudi, M. I., Monday, S. S., & Anthony, A. I. (2022). Human health risk assessment of heavy metals in drinking water sources in three senatorial districts of Anambra State, Nigeria. *Toxicology Reports*, *9*, 869. https://doi.org/10.1016/j.toxrep.2022.04.011.

[8] Briffa, J., Sinagra, E., & Blundell, R. (2020b). Heavy metal pollution in the environment and their toxicological effects on humans. *Heliyon*, *6*(9), e04691.

[9] Bobaker, A. M., Alakili, I., Sarmani, S. B., Al-Ansari, N., & Yaseen, Z. M. (2019). Determination and Assessment of the Toxic Heavy Metal Elements Abstracted from the Traditional Plant Cosmetics and Medical Remedies: Case Study of Libya. *International Journal of Environmental Research and Public Health*, *16*(11), 1957. https://doi.org/10.3390/ijerph16111957 .

[10] WHO (World Health Organization). (2018) "Stop lead poisoning in children", http://www/who. Int/media Centre/news/notes/2013/lead.

[11] USEPA. (2018). (United States Environmental Protection Agency), "Highlights of the Exposure Factors Handbook (Final Report) U.S. Environmental Protection Agency, Washington, DC, EPA/600/R-18/030. Service, 2018.

[12] Otugboyega, J., Madu, F., Otugboyega, O., Ayomipo, O., Adeyeye, J., & Ajayi, J. (2023). Biomonitoring and Biomathematical Modeling of Health Risks Associated with Dumpsite Grown Vegetables in Lagos State. *Biological Trace Element Research*, *202*, 1–16. https://doi.org/10.1007/s12011-023-03903-w.

[13] Nicholas, E. S., Ukoha, P. O., & Ihedioha, J. N. (2024). Comparative assessment of the effect of storage vessels, thatched roof and industrial activity on harvested rainwater quality in south eastern, Nigeria using water quality index. *Discover Water*, *4*(1), 42. https://doi.org/10.1007/s43832-024-00081-1

[14] Torrieri, E., Pepe, O., Ventorino, V., Masi, P., & Cavella, S. (2014a). Effect of sourdough at different concentrations on quality and shelf life of bread. *LWT - Food Science and Technology*, *56*(2), 508–516. https://doi.org/10.1016/j.lwt.2013.12.005.

[15] Isaac, E., Maitera, O. N., Donatus, R. B., Riki, Y. E., Yerima, E. A., Tadzabia, K., & Joseph, B. (2019). Energy dispersive X-Ray fluorescence determination of minor and major elements in soils of Mambilla Plateau Northeastern Nigeria. *Journal of Environmental Chemistry and Ecotoxicology*, *11*(2), 22–28. https://doi.org/10.5897/JECE2018.0442.

[16] Khan, R., Anwar, F., & Ghazali, F. M. (2024a). A comprehensive review of mycotoxins: Toxicology, detection, and effective mitigation approaches. *Heliyon*, *10*(8), e28361. https://doi.org/10.1016/j.heliyon.2024.e28361

Bayero Journal of Physics and Mathematical Sciences / Vol. 16, No. 1 / March, 2025. ISSN: 1597 – 9342, Online ISSN: 2795 - 3866

BAJOPMAS JOURNAL 16(1): 155 – 166
Printed in Bayero University, Kano - Nigeria.

SYNTHESIS AND CHARACTERIZATION OF EARTH METAL OXIDE NANOPARTICLES FOR SOLAR THERMAL APPLICATION

[*1]Umar, Y and Darma, T. H.
[1]Department of Applied Physics, School of Applied Sciences, Federal Polytechnic Nasarawa, Nigeria.
[2] Department of Physics, Faculty of Physical Sciences, Bayero University Kano, Nigeria.
*Corresponding Author:
[1]Department of Applied Physics, School of Applied Sciences, Federal Polytechnic Nasarawa, Nigeria
Email: uyakubu2017@gmail.com; Phone number: +2348039635596

ABSTRACT
Metal oxides are a promising class of materials for solar thermal applications due to their excellent light absorption, thermal stability, and ease of synthesis. When produced in nano size, metal oxides have been recognized as suitable materials for improving thermo-physical properties of working fluids or coatings in solar thermal applications. In this research, earth metal oxides of Aluminium oxide (Al_2O_3), Nickel oxide (NiO) and Antimony oxide (Sb_2O_3) nanoparticles were synthesized using suitable precursors which include Aluminium nitrate, $Al(NO_3)_3.9H_2O$, Nickel Chloride, $NiCl_2.6H_2O$, Antimony chloride ($SbCl_3$) and Urea, $CO(NH_2)_2$ respectively, in de-ionized water as based fluid by Hydrothermal method. The synthesized Al_2O_3 nanoparticles was obtained by calcination of the intermediate product, Aluminium hydroxide, (AlOOH) precipitate from the hydrothermal process at 1000^{o}C for 4 hours. NiO nanoparticles was obtained by annealing Nickel hydroxide, Ni(OH) of the synthesized product at 400^{o}C for 3 hours and Sb_2O_3 nanoparticles was obtained by heating Antimony oxychloride, (SbOCl) from the hydrothermal process at 60^{o}C for 4 hours. Their crystal structure and surface morphology were characterized by employing X-ray diffraction (XRD) and Field Emission Scanning Electron Microscopy (FESEM) techniques to ascertain their purity. From the XRD results of the analysis of Al_2O_3 nanoparticles showed the main diffraction peaks at 2θ = 32.783^o, 67.418^o, 36.684^o, 31.207^o, 32.783^o and 44.796^o which is in agreement with the International center for Diffraction Data (ICDD) standard pattern Ref. card no. 98-003-7392 and monoclinic in nature as seen from the crystallographic parameter, with crystallite size evaluated as 14.2nm (Debye Scherrer method). For NiO nanoparticles, the results of the analysis described the main diffraction peaks at 2θ = 43.254^o, 37.227^o, 62.829^o, 75.352^o and 79.341^o respectively, this is also in agreement with the International center for Diffraction Data (ICDD) standard pattern Ref. card no. 98-000-8170 and cubic in nature as describe by the crystallographic parameter, its crystallite size was calculated as 9.5nm (Debye Scherrer method). The XRD results of the analysis of Sb_2O_3 nanoparticles indicate the main diffraction peaks at 2θ = 27.718^o, 46.053^o, 54.603^o, and 32.112^o respectively which is equally in agreement with the International center for Diffraction Data (ICDD) standard pattern Ref. card no. 98-001-7507 and cubic in nature as obtained from the crystallographic parameter, with crystallite size determined as 32.22nm (Debye Scherrer method). The FESEM surface morphology for the samples revealed the distribution peaks as unimodal, having one main peak suggesting all samples are relatively uniform in size having a diameter of 64.2nm, 50.1nm, and 8.8nm for Al_2O_3, NiO and Sb_2O_3 respectively. The Crystal structure, crystallite size and surface morphology give rise to greater surface area and can greatly influence heat capacity and absorption by nanoparticles in a based fluid, hence the results shows that the synthesized nanoparticles can offer high thermal conductivity and excellent thermal stability, making them promising candidates for efficient solar energy absorption suitable for solar thermal application.

Keywords: Earth Metal Oxides, Nanoparticles, Solar energy, Solar thermal collector.

1.0 Introduction
Solar thermal collectors are targeted to operate at high temperature to give high thermal efficiency, but the huge amount of flux incident on the conventional solar collector causes

large temperature difference and high thermal resistance between the solar coating surface and the working fluid, degrading the performance of the solar thermal collector over time [1] and [2].

Recent researches have shown that heat transfer fluids containing nanoparticles (nanofluids) have great potential in harnessing solar energy [3]. Metal oxides are a promising class of materials for solar thermal applications due to their excellent light absorption, thermal stability, low poisonousness and ease of synthesis [4].

Crystal structure, crystallite size and surface morphology are some of the factors that gave rise to greater surface area and can greatly influence heat capacity and absorption by nanoparticles in a based fluid [5]. This shows that metal oxide nanoparticles can offer high thermal conductivity and excellent thermal stability, making them promising candidates for efficient solar energy storage [6].

The synthesis and characterization of metal oxide nanoparticles is essential for understanding their structural and rheological properties [7]. Techniques such as X-ray diffraction (XRD), Field Emission Scanning Electron Microscopy (FESEM) and UV-Visible spectroscopy are commonly used to analyze the crystallinity, size and optical properties of metal oxide nanoparticles in nanofluids [8]. By employing a combination of these characterization techniques, valuable insights into the fundamental properties of the metal oxide nanoparticles for solar thermal applications were achieved [9].

2.0 Theoretical Background

By understanding the theoretical concepts of light-matter interaction and employing the characterization techniques with their relevant equations and the specific synthesis methods chosen, were targeted to optimize the metal oxide nanoparticles (Al_2O_3, NiO, Sb_2O_3) for efficient solar thermal applications.

2.1 X-ray Diffraction: XRD is one of the most important characterization techniques to reveal the structural properties of nanoparticles. It gives enough information about the crystallinity and phase of NPs. It also provides rough idea about the particle size through Debye Scherer formula [10].

XRD uses X-rays to determine the crystal structure and phase composition of a material. Bragg's equation is given by

$$n\lambda = 2dsin\theta \quad (1)$$

where: n is an integer, λ is the X-ray wavelength, d is the interplanar spacing, and θ is the diffraction angle [11]. The Scherrer's equation is given by

$$D(hkl) = \frac{k\lambda}{\beta cos\theta} \quad (2)$$

where: D: is the crystallize size (in nm), K ≈ 0.9 is dimensionless shape factor, λ = 1.5406Å, is the wavelength of the X-ray radiation, β: is the Full width at half maximum (FWHM) of the diffraction peak in radians, θ: is the Bragg angle in degree [12].

2.1.1 Field Emission Scanning Electron Microscopy (FESEM)

Field Emission Scanning Electron Microscopy (FESEM) was employed to assess the morphological properties of the materials.

2.1.2 Ultraviolet, Visible, and Near-Infrared (UV-Vis-NIR)

This technique measures the transmittance and absorption of light by a material across the (UV-Vis-NIR) spectrum [13].
Transmittance, T; By Beer- Lambert law [13].

If sample is transparent: $\%T = 100\%; I_\circ = I$ (3)

If sample is not transparent $\%T < 100\%; I_\circ \neq I$ (4)
where; I is the intensity of transmitted light through sample solution, $I_\circ$ is the intensity of incident light

Absorbance; By Beer- Lambert law [14].

Absorbance, $A = \log 10 \frac{1}{T}$ (5)

where: $\log 10$ presents the base-10 logarithm

Energy of Photon, $E = \frac{h\nu}{\lambda} = \frac{1240}{\lambda}$ (6)

where: h is Planck's constant, ν speed of light and λ wavelength of light [14].

Absorption coefficient, $\alpha = 2.303 \times \frac{A}{d}$ (7)

where: A is absorbance, d is the path length of light through the sample

2.1.3 Zeta Potential: Zeta potential measures the surface charge of nanoparticles in a suspension. It influences the stability of the nanofluid by preventing particle aggregation [15].

2.1.4 Particle Size: Particle size significantly impacts a nanofluid's properties. Smaller particle size generally leads to better heat transfer due to increased surface area for interaction with the base fluid-de-ionized water, [16].

2.2 Review of Related works

Some studies had been reported in using nanoparticles in base fluids as nanofluids in solar energy storage.

[17] elucidated that Al_2O_3 nanoparticles exhibiting a theta phase spherical crystalline structure were successfully synthesized employing a self-combustion technique utilizing bauxite and sugar as the principal raw materials. The resultant self-combustion product underwent calcination at 1200°C for duration of 4 hours, and the X-ray diffraction (XRD) analysis indicated that the crystallite size of the Al_2O_3 nanoparticles was determined to be 15.5 nm, whereas the surface morphology assessed through transmission electron microscopy (TEM) analysis indicated that the average particle size was 30 nm.

[18] documented the successful synthesis of copper oxide (CuO) and aluminium oxide (Al_2O_3) utilizing a two-step method combining various routes. A total of 2.3 grams of copper nitrate, $Cu(NO_3)_3$, along with 0.83 grams of glycine, were solubilized in a minimal volume of double distilled water. Similarly, 4.25 grams of aluminium nitrate, $Al(NO_3)_3$, combined with 0.83 grams of glycine, were dissolved in a sufficient quantity of double distilled water. The resultant distinct solutions yielded a foam product composed of CuO and Al_2O_3, along with their associated by-products. The foam products underwent calcination at approximately 800°C for duration of six hours. The X-ray diffraction (XRD) analysis of the CuO nanoparticles demonstrated a remarkable degree of crystallinity of the synthesized material, with a crystallite size measured at 32 nm. The Al_2O_3 nanoparticles exhibited a rhombohedral lattice structure, thereby affirming their superior crystal quality with a crystallite size of 18 nm.

[6] elucidated that aluminum oxide (Al_2O_3) nanoparticles exhibiting a gamma crystal structure were effectively synthesized employing the hydrothermal technique, utilizing aluminum chloride ($AlCl_3$) and urea $CO(NH_2)_2$ as the primary precursors. The synthesis was conducted at a temperature of 170°C for duration of 17 hours. Subsequently, the hydrothermal product underwent calcination at 500°C for one hour. The resultant Al_2O_3 nanoparticles were characterized utilizing X-ray diffraction (XRD) and Transmission Electron Microscopy (TEM). The XRD analysis indicated that the synthesized nanoparticles corresponded to gamma-alumina (γ-Al_2O_3), possessing a crystallite size of 4 nm. The TEM imagery revealed an aggregation of rod-like particles with an average diameter of 6 nm, which was significantly influenced by the presence of urea as a capping agent. The Al_2O_3 nanoparticles produced possess the capability to generate highly stable nanofluids, which hold considerable promise for applications in energy storage systems.

[19] elucidated that Nickel oxide nanoparticles were generated through hydrothermal methodologies employing Nickel Nitrate, $Ni(NO_2).6H_2O$, Urea, $CO(NH_2)_2$, and Citric acid, which were solubilized in a 1:1 ratio of 1,2 propanediol to water. The resultant synthesized material underwent a drying process at a temperature of 400^{o}C for a duration of four hours. The X-ray diffraction (XRD) analysis indicated that the NiO nanoparticles exhibited pronounced ring patterns attributable to a hexagonal lattice structure, thereby suggesting a high degree of crystallinity in the obtained sample.

Dhas *et al*. (2020) elucidated that porous NiO particles were fabricated utilizing the hydrothermal technique, employing Nickel Acetate, $Ni(CH_3CO_2)_2.4H_2O$, with methanol serving as the primary solvent dissolved in double distilled water. The resultant hydrothermal product underwent calcination at a temperature of 350^{o}C for a duration of 2 hours in an atmospheric environment. The X-ray diffraction (XRD) analysis indicated that the synthesized NiO nanoparticles exhibit a monoclinic crystalline structure, signifying a high degree of crystallinity of the resultant material, with an average crystallite size measured at 9.3 nm.

[20] detailed the creation of alpha-aluminum oxide (α-Al_2O_3) and gamma-aluminum oxide (γ-Al_2O_3) nanoparticles. They employed an auto-combustion technique, dissolving aluminum nitrate and glycine in water as their starting materials. By controlling the calcination temperature, they selectively produced different aluminum oxide phases: 800°C yielded γ-Al_2O_3 nanoparticles, while 1000°C resulted in α-Al_2O_3 nanoparticles. X-ray diffraction (XRD) analysis revealed that the γ-Al_2O_3 nanoparticles had an average crystallite size of 5.8 nm, and the α-Al_2O_3 nanoparticles measured 15 nm. Notably, the nanoparticles exhibited minimal clumping, suggesting their potential for use in stable nanofluids suitable for energy storage applications.

[20] used an ultrasound-assisted co-precipitation method to create iron(III) oxide (Fe_3O_4) nanoparticles. They mixed iron (III) chloride ($FeCl_3$) and iron(II) sulfate heptahydrate ($FeSO_4 \cdot 7H_2O$) as their starting materials, and then precipitated the Fe_3O_4 by slowly adding sodium hydroxide (NaOH) solution. After filtering, washing, and drying the resulting powder, they confirmed the formation of Fe_3O_4 using XRD, TEM, and UV-vis spectroscopy. XRD analysis showed the nanoparticles had a cubic spinel structure with a crystalline size of about 26 nm. TEM images revealed the nanoparticles were spherical and varied in size, with an average particle size of approximately 12 nm.

[20] synthesized cobalt oxide (Co_3O_4) nanoparticles via a sol-gel method, varying both pH and annealing temperature. They dissolved cobalt (II) nitrate hexahydrate in a water-

isopropyl alcohol mixture, adjusting the pH to 8, 10, 12, and 14, and then annealed the resulting products at 400°C, 600°C, and 800°C.

pH 8: Samples annealed at 120°C, 400°C, and 600°C were amorphous. At 800°C, crystalline $Co_3 O_4$ formed, with a crystallite size of 46.6 nm.
pH 10: The 120°C sample was amorphous. At 400°C, crystallinity appeared. Annealing at 600°C and 800°C yielded crystalline $Co_3 O_4$ with crystallite sizes of 23.3 nm and 34.9 nm, respectively.

pH 12: The 120°C sample was amorphous. At 400°C and 600°C, crystalline $Co_3 O_4$ formed, with crystallite sizes of 11.6 nm and 23.3 nm, respectively. At 800°C, a more complex crystalline structure emerged, with a crystallite size of 32.57 nm.
pH 14: Samples annealed at 120°C and 400°C showed similar crystallite sizes of 23.3 nm. At 800°C, the crystallite size was 34.85 nm.

In essence, the study demonstrated that both pH and annealing temperature significantly influenced the crystallinity and crystallite size of the synthesized $Co_3 O_4$ nanoparticles.
Keneshbekova *et al.* (2023) synthesized $Co_3 O_4$ nanoparticles via solution combustion, using cobalt nitrate, glycine, and nitric acid. They dissolved these reagents in water, heated the solution to 260°C, which triggered a rapid temperature increase to 1200°C and nanoparticle formation. The resulting product was washed and dried. Scanning electron microscopy showed that:

A 1:2 stoichiometric ratios (cobalt nitrate to glycine) yielded nanoparticles ranging from 23 to 60 nm, but with significant clumping, likely due to the high combustion temperature fluctuations.
A 1:3 ratio produced nanoparticles ranging from 20 to 65 nm, with noticeably less agglomeration.
The study concluded that varying the initial reagent ratios effectively alters the $Co_3 O_4$ nanoparticle morphology, demonstrating the potential for controlled synthesis.

Synthesized pure and copper-doped titanium dioxide (TiO_2) nanoparticles using a co-precipitation method. They mixed titanium tetraisopropoxide (TTIP) and ethanol, then added sodium hydroxide to achieve a pH of 10. The resulting precipitate was washed, dried, and annealed. XRD analysis showed the TiO_2 nanoparticles had an anatase phase with a tetragonal crystal structure. The pure TiO_2 had a crystallite size of 10.9 nm. Copper doping at concentrations of 0.025M, 0.05M, 0.075M, and 0.1M resulted in progressively smaller crystallite sizes: 10.2 nm, 9.1 nm, 8.3 nm, and 7.9 nm, respectively, indicating a concentration-dependent effect likely due to copper's amphoteric nature. SEM images revealed that both pure and copper-doped TiO_2 nanoparticles had particle sizes ranging from 25 to 40 nm.

The synthesized nanoparticles demonstrate potential for applications in dye-sensitized solar cells (DSSCs) and photocatalysis, due to their light-harvesting and catalytic properties.

The reported XRD and surface morphology analyses of the synthesized nanoparticles indicate that their physical characteristics have been altered, leading to nanoparticles capable of forming exceptionally stable nanofluids. These nanofluids show promise for applications in energy storage systems.

The Sb_2O_3 nanoparticles, synthesized via a hydrothermal process and annealed at 550°C for 24 hours, exhibit a particle size of 32.24 nm, which closely aligns with the findings of [21].

Their study produced antimony-tin oxide nanoparticles using a similar hydrothermal method, annealing at 600°C, and reported a crystallite size of 32.24 nm. This paper presented the synthesis and characterization of metal oxides of Aluminium oxide (Al_2O_3), Nickel oxide (NiO) and Antimony oxide (Sb_2O_3) nanoparticles which aims to advanced their understanding, efficiency and potential for harvesting large amount of solar energy for solar thermal application.

3.0 Materials and Method

In this research the main materials involve the use of suitable precursors such as Aluminium nitrate, $Al(NO_3)_3.9H_2O$, Nickel Chloride, $NiCl_2.6H_2O$, Antimony chloride ($SbCl_3$), Urea, $CO(NH_2)_2$, distilled water and de-ionized water.

3.1 Method

In this study the synthesis method was restricted to Hydrothermal method.
Aluminum oxide (Al_2O_3) nanoparticles were synthesized using a hydrothermal method. The process involved dissolving 1.1253g of Aluminium nitrate, $Al(NO_3)_3.9H_2O$, and 0.36036g of Urea, $CO(NH_2)_2$, in 100ml of distilled water under vigorous magnetic stirring for 30 minutes. The mixture was then placed in a Teflon-lined stainless steel autoclave and maintained at 160^{o}C for 3 hours and air cooled overnight. A white aluminium hydroxide (AlOOH) precipitate was obtained, washed with distilled water using centrifugal machine at 3000 revolutions per minute (rpm). and anhydrous alcohol to remove residual contaminants, dried in an oven at 80^{o}C for 12 hours, crushed using mortar and pistil after thorough cleaning, and taken into an LT 100 Furnace for calcination at 1000^{o}C for 4 hours.

Nickel oxide (NiO) nanoparticles were synthesized using a similar method. 2.377g of Nickel Chloride, $NiCl_2.6H_2O$, was dissolved in 100ml beaker containing 20ml of deionized water, then 10ml of prepared Urea, $CO(NH_2)_2$ solution was added dropwise under vigorous magnetic stirring for 30 minutes at room temperature until all $NiCl_2.6H_2O$ particles were completely dissolved. The mixed solution was transferred into a Teflon-lined stainless steel autoclave and maintained under heated temperatures of 110^{o}C for 6 hours. A greenish nickel hydroxide (NiOH) precipitate was obtained, washed with deionized water using centrifugal machine at 3000 revolutions per minute (rpm) and ethanol to eliminate residual contaminants, dried in an oven at 70^{o}C for 12 hours, crushed using mortar and pistil, and taken into an LT 100 Furnace for annealing at 400^{o}C for 3 hours, resulting in a black color powder.

Antimony oxide (Sb_2O_3) nanoparticles were prepared via a hydrothermal method. 0.005mol of $SbCl_3$ was added to 45ml of distilled water in a beaker at room temperature under continuous stirring. To prevent the $SbCl_3$ solution from hydrolyzing, an appropriate amount of ammonia was dripped inside. The mixture was further put under continuous magnetic stirring for 40 minutes to form a heterogeneous mixture with white insoluble precipitate and then transferred to a 60ml Teflon-lined stainless autoclave. The autoclave was sealed and placed in an oven at temperature of 150^{o}C for 2 hours. The resulting white solid product was filtered, washed with distilled water and alcohol. The sample was dried in a vacuum at 60^{o}C for 4 hours and calcined at 550^{o}C for 24 hours, the resulting powder was collected for characterization.

3.1.1 Characterization of metal oxide nanoparticles

All the metal oxides were characterized using X-ray diffraction (XRD) machine, X'pert Pro Panalytical PW MPD in the range 10^o - 80^o with Cu-Kα (λ = 1.5406Å) as radiation source to

confirmed crystallinity and phase purity of the synthesized nanoparticles. The analysis was performed using X'pert HighScore Plus software.

For surface morphology of the synthesized metal oxide nanoparticles, a Field Emission Scanning Electron Microscope was employed using TESCAN CLARA E-T, AXIAL.

4.0 Results

4.1.0 XRD analysis of Al_2O_3

The visual appearance of Al_2O_3 powder nanoparticles synthesized in this study appear pure white. The powder was investigated by X-ray diffraction, using X-ray diffractometer (X'PERT PRO PANALYTICAL PW 3040 MPD model) with Cu-Kα radiation source (λ=1.5406Å) in the range 2θ = 10 - 80° to identify the phases and the crystallinity of Al_2O_3 calcined sample. The analysis of the raw data was performed using X'pertHighScore Plus software. The result of the analysis of Al_2O_3 nanoparticles is shown in Figure 1. The main diffraction peaks are seen at 2θ = 32.783°, 67.418°, 36.684°, 31.207°, 32.783° and 44.796° respectively, and they are very much in accordance with the standard ICDD diffraction pattern No. 98-003-7392. The diffraction peaks at 2θ = 32.783°, 67.418°, 36.684°, 31.207° and 32.783° corresponds to the planes (2 0 -2), (5 1 2), (1 1 1), (4 0 0) and (1 1 -2) respectively. The crystallite size was found to be 14.2nm (Debye Scherrer method). Also from the crystallographic parameter obtain from the X'pertHighScore Plus software, the shape of the Al_2O_3 sample is monoclinic in nature which can significantly influence its physical properties, particularly in terms of thermal stability in nanofluids.

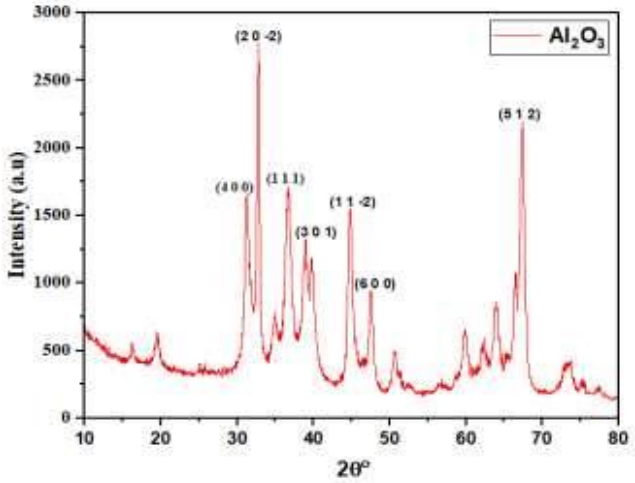

Fig. 1 Synthesized Al_2O_3 XRD Graph

4.1.1 XRD analysis of NiO

The physical appearance of NiO powder nanoparticles synthesized in this study appear black. The powder was investigated by X-ray diffraction, using X-ray diffractometer (X'PERT PRO PANALYTICAL PW 3040 MPD model) with Cu-Kα radiation source (λ=1.5406Å) in the range 2θ = 20 - 80° to identify the phases and the crystallinity of NiO annealed sample. The analysis of the raw data was performed using X'pertHighScore Plus software. The result of the analysis of NiO nanoparticles in shown in Figure 2. The main diffraction peaks are seen at 2θ = 43.254°, 37.227°, 62.829°, 75.352° and 79.341° respectively and they are very much in accordance with the standard ICDD diffraction pattern No. 98-000-8170. The diffraction peaks at 2θ = 43.254°, 37.227°, 62.829°, 75.352° and 79.341° corresponds to the planes (0 0 2), (1 1 1), (0 2 2), (1 1 3) and (2 2 2) respectively. The crystallite size was found to be

9.5nm (Debye Scherrer method). From the crystallographic parameter as indicated from the X'pertHighScore Plus software, the shape of the NiO sample is cubic, which is essential for its stability and performance in nanofluids applications.

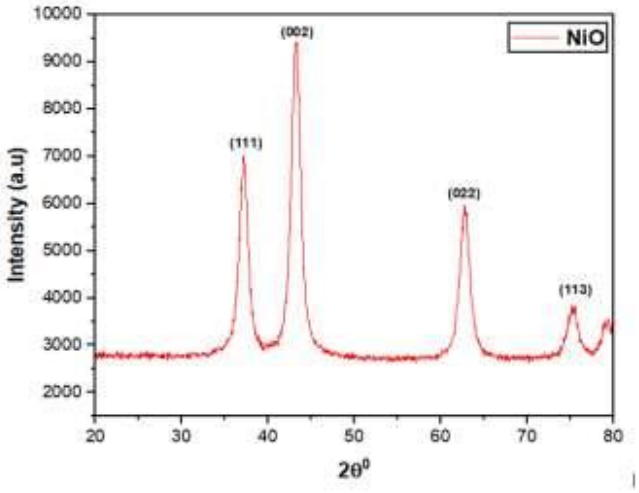

Fig. 2 Synthesized NiO XRD Graph

4.1.2 XRD analysis of Sb_2O_3

The appearance of Sb_2O_3 powder nanoparticles synthesized in this study appear pure white. The powder was investigated by X-ray diffraction, using X-ray diffractometer (X'PERT PRO PANALYTICAL PW 3040 MPD model) with Cu-Kα radiation source (λ=1.5406Å) in the range 2θ = 20 - 80° to identify the phases and the crystallinity of Sb_2O_3 heated sample. The analysis of the raw data was performed using X'pertHighScore Plus software. The result of the analysis of Sb_2O_3 nanoparticles is shown in Figure 3. The main diffraction peaks are seen at 2θ = 27.718°, 46.053°, 54.603°, and 32.112° respectively and they are very much in accordance with the standard ICDD diffraction pattern Ref. No. 98-001-7507. The diffraction peaks at 2θ = 27.718°, 46.053°, 54.603°, and 32.112° corresponds to the planes (2 2 2), (0 4 4), (2 2 6), and (0 0 4) respectively. The crystallite size was found to be 32.22nm (Debye Scherrer method). Also from the crystallographic parameter as indicated from the X'pertHighScore Plus software, the shape of the Sb_2O_3 sample is cubic, specifically the senarmontite cubic phase synthesized, exhibits unique characteristics that enhance its applicability in various fields, including electronics and energy storage.

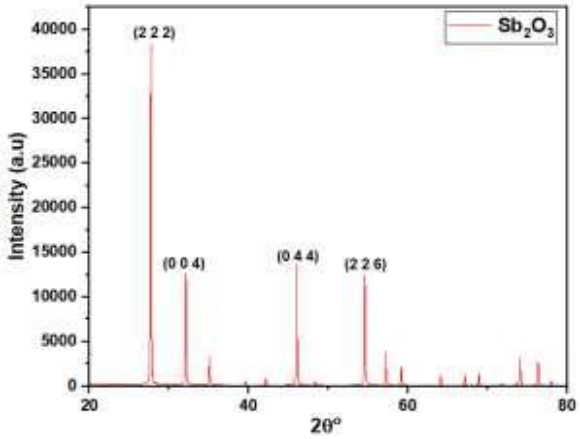

Fig. 3 Synthesized Sb_2O_3 XRD Graph

4.2 Morphological Analysis of the synthesized samples.

The surface morphology for the samples revealed the distribution peaks as unimodal, having one main peak suggesting all samples are relatively uniform in size having a diameter of 64.2nm, 50.1nm, and 8.8nm as shown in figure 4, 5 and 6 for Al_2O_3, NiO and Sb_2O_3 respectively.

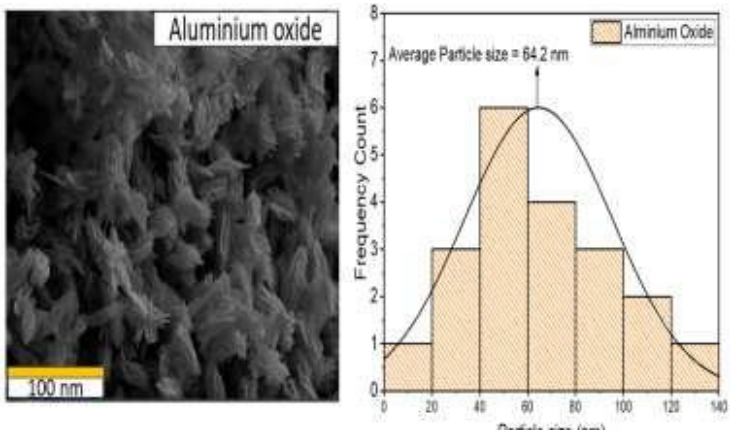

Fig. 4. FESEM image and Histogram of synthesized Al_2O3 nanopartcles

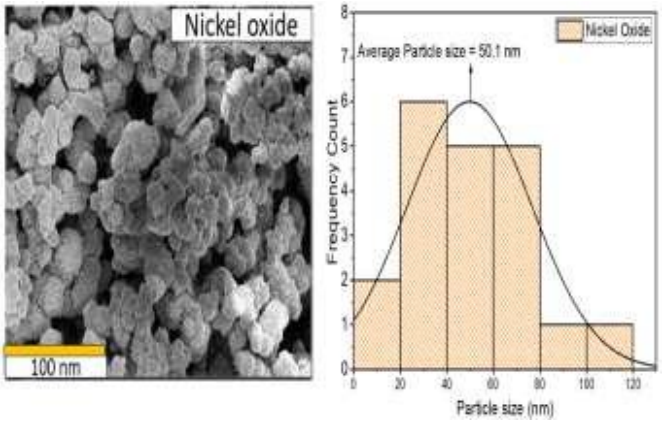

Fig. 5. FESEM image and Histogram of synthesized NiO nanopartc

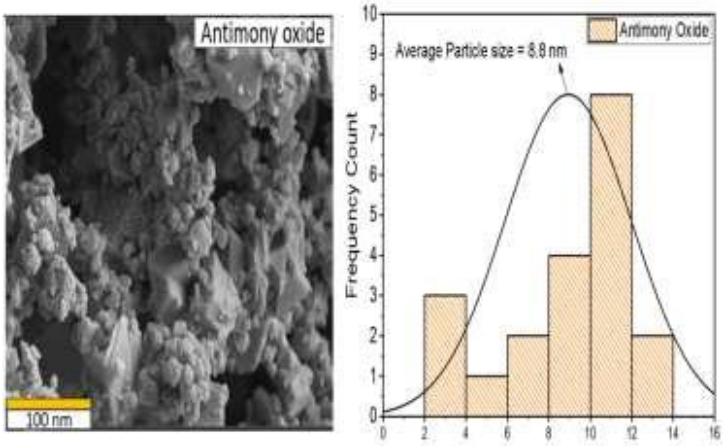

Fig. 4. FESEM image and Histogram of synthesized Sb_2O3 nanopartcles

5.0 Conclusion

This study successfully created aluminum oxide ($Al_2 O_3$), nickel oxide (NiO), and antimony oxide ($Sb_2 O_3$) nanoparticles using a hydrothermal method.

The X-ray diffraction (XRD) confirmed the purity and specific crystal structures of each nanoparticle, matching standard database patterns. Scherrer's equation was used to determine the crystallite sizes: 14.2 nm for $Al_2 O_3$, 9.2 nm for NiO, and 32.22 nm for $Sb_2 O_3$.

$Al_2 O_3$ was found to be monoclinic, while NiO and $Sb_2 O_3$ were cubic, indicating their good crystallite size. Field Emission Scanning Electron Microscopy (FESEM) revealed uniform particle distribution, with average diameters of 64.2 nm for NiO, and 8.8 nm for $Sb_2 O_3$.

The $Al_2 O_3$ results were comparable to studies using self- and auto-combustion methods [17] and [5].
The NiO crystallite size was similar to that obtained in another hydrothermal synthesis [20].

The Sb_2O_3 crystallite size was comparable to Antimony-tin oxide nanoparticles created by hydrothermal methods [21]. The study also compared the crystallite sizes to a study that doped TiO_2 with copper, demonstrating the effect of doping on crystallite size [21].

The crystal structure, crystallite size, and surface morphology of the synthesized nanoparticles contribute to a large surface area. These properties enhance heat capacity and absorption, suggesting the nanoparticles can provide high thermal conductivity and stability.

Therefore, these nanoparticles are promising materials for efficient solar energy absorption in solar thermal applications.

Contribution to Knowledge

This research successfully created and analyzed aluminum oxide ($Al_2 O_3$), nickel oxide (NiO), and antimony oxide ($Sb_2 O_3$) nanoparticles using a hydrothermal method. By comparing the findings, particularly crystallite size and surface morphology, with existing studies, the work demonstrates the potential of these nanoparticles for efficient solar energy harvesting. This approach offers an alternative solution for solar collectors in renewable energy, thereby contributing to efforts to mitigate climate change and foster environmental sustainability.

Acknowledgement

I wish to appreciate the Department of Physics, Universiti Putra Malaysia (UPM) for procuring all the reagents used for this research via TETFUND grant and most of the equipment used for synthesis and characterization of the metal oxide samples for XRD, FESEM, UV-Vis, Zeta Potential and Particle size in collaboration with Institute of Nanoscience and Nanotechnology (ION2), Institute of Biosciences (IBS) at UPM and other Research Organizations. I also acknowledge the Federal Government of Nigeria through Tertiary Education Trust Fund (TETFUND) for the sponsorship to go for this Research attachment.

REFERENCES

[1] Verma, S. K., Gupta, N. K., & Rakshit, D. (2020). A comprehensive analysis on advances in application of solar collectors considering design, process and working fluid parameters for solar to thermal conversion. Solar Energy, 208, 1114-1150. https://doi.org/10.1016/j.solener.2020.08.042

[2] Lipiński, W., Abbasi-Shavazi, E., Chen, J., Coventry, J., Hangi, M., Iyer, S., ... & Wheeler, V. M. (2021). Progress in heat transfer research for high-temperature solar thermal applications. *Applied Thermal Engineering*, *184*, 116137. https://doi.org/10.1016/j.applthermaleng.2020.116137

[3] Prabhu, S., Thangadurai, T. D., Bharathy, P. V., & Kalugasalam, P. (2022). Synthesis and characterization of nickel oxide nanoparticles using Clitoria ternatea flower extract: Photocatalytic dye degradation under sunlight and antibacterial activity applications. *Results in Chemistry*, *4*, 100285. https://doi.org/10.1016/j.rechem.2022.100285

[4] Rasheed, T., Hussain, T., Anwar, M. T., Ali, J., Rizwan, K., Bilal, M., & Almuslem, A. S. (2021). Hybrid nanofluids as renewable and sustainable colloidal suspensions for potential photovoltaic/thermal and solar energy applications. *Frontiers in Chemistry*, *9*, 737033. https://doi.org/10.3389/fchem.2021.737033

[5] Ahmed, M. I., Hossam, S. J., Hassan, A. D., and Mostafa, Y. N. (2021). "Synthesis and characterization of γ-Al_2O_3 and α-Al_2O3 nanoparticles using a facile, inexpensive auto-combustion approach." *Egyptian Journal of Chemistry* 64, no. 5: 2509-2515. https://doi.org/10.21608/ejchem.2021.61793.3330

[6] Dani, G. S., Djoko, H. P., & Jupiter, S. P. (2020). Hydrothermally synthesis of Al_2O_3 nanoparticles for nanofluids with enhanced Critical heat flux. In *Journal of Physics: Conference Series* (Vol. 1428, No. 1, p. 012023). IOP Publishing. https://doi.org/ 10.1088/1742-6596/1428/1/012023

[7] Yasmin, H., Giwa, S. O., Noor, S., & Sharifpur, M. (2023). Thermal conductivity enhancement of metal oxide nanofluids: A critical review. *Nanomaterials*, *13*(3), 597. https://doi.org/10.3390/nano13030597

[8] Carbone, M., Bauer, E. M., Micheli, L., & Missori, M. (2017). NiO morphology dependent optical and electrochemical properties. *Colloids and Surfaces A: Physicochemical and Engineering Aspects*, *532*, 178-182. https://doi.org/10.1016/j.colsurfa.2017.05.046

[9] Prakash, A., Satsangi, S., Mittal, S., Nigam, B., Mahto, P. K., & Swain, B. P. (2018, June). Investigation on Al_2O_3 nanoparticles for nanofluid applications-a review. In *IOP conference series: materials science and engineering* (Vol. 377, No. 1, p. 012175). IOP Publishing. https://doi.org/ 10.1088/1757-899X/377/1/012175

[10] Khan, I., Saeed, K., & Khan, I. (2019). Nanoparticles: Properties, applications and toxicities. *Arabian journal of chemistry*, *12*(7), 908-931. http://dx.doi.org/10.1016/j.arabjc.2017.05.011

[11] Ning, H., Guo, H., Zhang, J., Wang, X., Jia, X., Qiu, J., ... & Ding, J. (2021). Enhancing the efficiency of Sb_2S_3 solar cells using dual-functional potassium doping. *Solar Energy Materials and Solar Cells*, *221*, 110816. https://doi.org/10.1016/j.solmat.2020.110816

[12] Ismail, R. A., Zaidan, S. A., & Kadhim, R. M. (2017). Preparation and characterization of aluminum oxide nanoparticles by laser ablation in liquid as passivating and anti-reflection coating for silicon photodiodes. *Applied Nanoscience*, *7*, 477-487. https://doi.org/ 10.1007/s13204-017-0580-0

[13] Khalid, K., Ishak, R., & Chowdhury, Z. Z. (2024). UV–Vis spectroscopy in non-destructive testing. In *Non-destructive material characterization methods* (pp. 391-416). Elsevier. https://doi.org/10.1016/B978-0-323-91150-4.00021-5

[14] Mayerhöfer, T. G., Pahlow, S., & Popp, J. (2020). The Bouguer- Beer- Lambert law: Shining light on the obscure. *ChemPhysChem*, *21*(18), 2029-2046. **https://doi.org/10.1002/cphc.202000464**

[15] Singh, R. P., Sharma, K., & Mausam, K. (2020). Dispersion and stability of metal oxide nanoparticles in aqueous suspension: A review. *Materials Today: Proceedings*, *26*,

2021-2025. https://doi.org/10.1016/j.matpr.2020.02.439

[16] Das, P. K., Mallik, A. K., Molla, A. H., Santra, A. K., Ganguly, R., Saha, A., ... & Aswal, V. K. (2022). Experimental investigation for stability and surface properties of TiO_2 and Al_2O_3 water-based nanofluids. *Journal of Thermal Analysis and Calorimetry*, *147*(10), 5617-5635. https://doi.org/10.1007/s10973-021-10894-0

[17] Syarif, D. G., Yamin, M., & Pratiwi, Y. I. (2019). Self-combustion synthesis of Al_2O_3 nanoparticles from bauxite utilizing sugar as fuel for nanofluids with enhanced CHF. In *Journal of Physics: Conference Series* (Vol. 1153, No. 1, p. 012068). IOP Publishing. https://doi.org/10.1088/1742-6596/1153/1/012068

[18] Amalraj, S., & Michael, P. A. (2019). Synthesis and characterization of Al_2O_3 and CuO nanoparticles into nanofluids for solar panel applications. *Results in Physics*, *15*, 102797. https://doi.org/10.1016/j.rinp.2019.102797

[19] Cao, S., Peng, L., Han, T., Liu, B., Zhu, D., Zhao, C., ... & He, S. (2020). Hydrothermal synthesis of nanoparticles-assembled NiO microspheres and their sensing properties. *Physica E: low-dimensional systems and nanostructures*, *118*, 113655. https://doi.org/10.1016/j.physe.2019.113655

[20] Dhas, S. D., Maldar, P. S., Patil, M. D., Nagare, A. B., Waikar, M. R., Sonkawade, R. G., & Moholkar, A. V. (2020). Synthesis of NiO nanoparticles for supercapacitor application as an efficient electrode material. *Vacuum*, *181*, 109646. https://doi.org/10.1016/j.vacuum.2020.109646

[21] Amutha, E., Rajaduraipandian, S., Sivakavinesan, M., & Annadurai, G. (2023). Hydrothermal synthesis and characterization of the antimony–tin oxide nanomaterial and its application as a high-performance asymmetric supercapacitor, photocatalyst, and antibacterial agent. *Nanoscale Advances*, *5*(1), 255-267. DOI: 10.1039/D2NA00666A